Journal of Materials Chemistry A

Accepted Manuscript

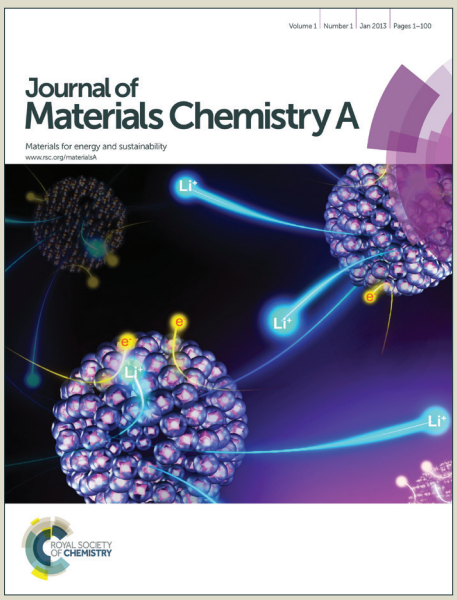

ROYAL SOCIETY OF CHEMISTRY

www.rsc.org/materialsA

Cite this: DOI: 10.1039/c0xx00000x

www.rsc.org/

COMMUNICATION

Hydrothermal Synthesis of Carbon-rich Graphitic Carbon Nitride Nanosheets for Photoredox Catalysis

Peng Zhang,[a,b,c] Xinghua Li,[a] Changlu Shao*,[a] Yichun Liu[a]

Received (in XXX, XXX) Xth XXXXXXXXX 20XX, Accepted Xth XXXXXXXXX 20XX

DOI: 10.1039/b000000x

We highlight a hydrothermal synthesis approach at low temperature to prepare the carbon-rich graphitic carbon nitride nanosheets, which show enhanced photocurrent and photocatalytic activity, due to its improved electron transport ability along the in-plane direction and increased lifetime of photoexcited charge carriers.

Graphitic carbon nitride (CN), a novel metal-free material, has attracted the attention of many scholars due to their special semiconductor properties and visible light absorption.[1] This cheap, easily available organic semiconductor has the smallest band gap among various carbon nitrides allotropes owing to the sp^2 hybridization of C and N atom, forming a solid-state aromatic system that is inert against most acids and bases. And, compared with the traditional metal and metal-oxide based materials, CN composed of carbon and nitrogen only are obviously ''sustainable'' and "environmentally friendly", which has been used in sustainable energy conversion and storage, direct methanol fuel cells, electrocatalysts and photocatalysis.[2] There is no doubt that CN and CN-based heterostructure has risen as a shining star in the horizon on the path of the scientists searching for new materials to meet future energy and environment demands. [3]

However, the practical performance of bulk CN is far from the ideal case which has been limited by several factors such as short lifetime of the excited-state carrier (10^{-12} s), poor oxygen evolution reaction (OER) kinetics and short hole diffusion length (2-4 nm).[4] Therefore, two-dimensional CN nanosheets with extremely small thickness in nanometer scale leading to exceptional electronic, thermal, mechanical, optical properties have attracted intensive interest. The apparent advantages associated with nanosheets include large specific surface area for providing abundant reactive sites for reducing the recombination probability of photoexcited charge carriers. The underlying but probably more important advantages are the shorter bulk diffusion length produced by monodisperse nanosheets with ultrathin thickness, which plays an important role in prolonging the lifetime of charge carriers and improve the quantum yield.

Up to now, CN materials were usually prepared by solid-state synthesis at high temperature.[1-5] However, the CN obtained through this method is bulk. In order to arrive at CN nanosheets with ultrathin thickness, bulk CN have to be further isolated through "thermal oxidation exfoliation" or "liquid exfoliation" routes.[5] The "thermal oxidation exfoliation" means a layer-by-layer thermal oxidation etching process of bulk CN in air, which brings out high cost and low yields. More importantly, the solid-state exfoliation might destroy the crystallization of CN by introducing large defects. While the "liquid exfoliation" means solvent as a blocker could enlarge the distance of layers by destroy the van der Waals force between C-N layers, which is hard to control to arrive at monodisperse nanosheets with high purity. Therefore, it is highly challenging but desirable to develop a direct effective approach for fabricating CN nanosheets of high quality in a controlled manner. Notably, soft chemistry solution-processing methods at low temperature are especially attractive, because they enable rational bottom-up design of novel functional nanomaterial by using solution assembly, crystallization and molecular engineering. Especially, benefitting from the versatile selection of reactant and reaction conditions, hydrothermal synthesis, chemical reactions carried out in "green" water solution, is widely applied to generate different kinds of nanosheets materials (e.g. metal oxides, sulfide and graphene). [6] It is therefore feasible to design a hydrothermal-assembly reaction to engineer the carbon nitrides precursors into CN nanosheet with 2D conjugated structures.[7]

Melamine (MA) is a universal and direct monomer source to synthesize CN, while the high bond energy of the chemical

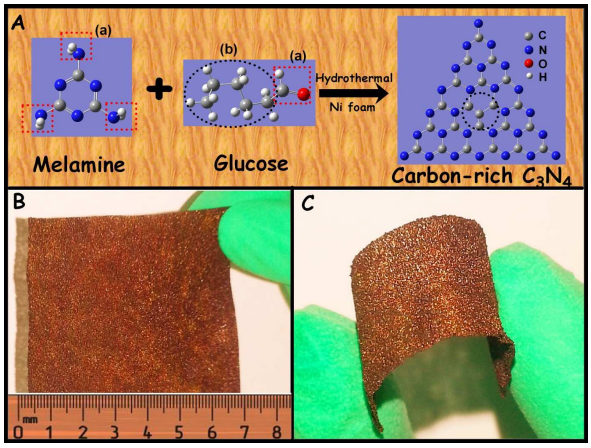

Fig. 1 (A) Polymerization processes of melamine (MA) and glucose in water solution.; (B,C) Demonstration of the CCN on nickel foam.

bond between melon units and -NH_2 groups of MA make it inactive in the low-temperature, catalyst-free and no other reactant, unfacilitating the condensation reaction of melon to form CN (Fig. 1). Notably, glucose is composed of aldehyde (-CHO) and six carbon hydroxyl (C–OH). The aldehyde (-CHO) of glucose and the amino (-NH_2) of MA might exist interaction in hydrothermal, which might weak and break the chemical bond between melon units and -NH_2. As a result, the obtained melon active units might be condensed to form CN. Meanwhile, carbon hydroxyl of glucose might be carbonized,[7] forming aromatic carbon banded with the as-formed CN framework by means of donor-accepter interactions. Therefore, glucose is expected to a promising alternative to assist constructing a complete 2D carbon-rich CN structure in a cooperative process, thus enabling their promising electrons transfer and photochemical application.[9]

Herein, we advanced a "green" water-solution synthesis of the novel carbon-rich graphitic carbon nitride nanosheet (CCN) using MA and glucose. Especially, the aldehyde (-CHO) and carbon hydroxyl (C–OH) of glucose make a reaction with MA in a cooperative process, which are in charge of the complete 2D carbon-rich CN structure. The details of the catalyst-free synthesis are described in the experimental section in the ESI†. For comparison, CN was also synthesized by heating MA at 550°C. Especially, due to the introduction of carbon doped in CN framework, two advantages are found in CCN: (a) Increased electrical conductivity because delocalized big π bonds among the carbons favor the electrons transfer; (b) Enhanced light absorption wavelength because of the narrower band gap. And, the as-prepared CCN nanosheets exhibited enhancement of photocurrent and photocatalytic activity. Considering the convenient and efficiency of practical application in photocatalytic and photovoltaic materials, nickel foam substrate as a self-sacrifice material was used to assist preparing and supporting CN nanosheet. And, it's interesting to note that the CN nanosheet self-assembled on nickel foam substrate is flexible and soft, as shown in Fig.1 (B, C), which would be favor of the separation, recovery and reuse of the catalysts.

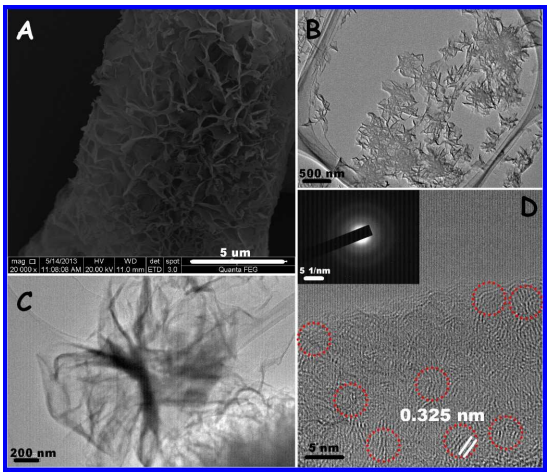

Fig. 2 (A) SEM image of CCN on nickel foam substrate; (B, C) TEM image of CCN at increasing magnification on copper mesh; (D) HRTEM image of CCN (Inset: SAED image of CCN).

Representative scanning electron microscopy (SEM) images (Figure 2A) of as-synthesized sample reveals a uniform layered morphology, unlike the parent bulk material consisting of solid agglomerates with a size of several micrometers (Figure S1). The molar ratio of C/N was shown in Table S1. Also, the nearly transparent feature of the nanosheets indicates its ultrathin thickness. From the AFM image (Figure S2), the thickness of the CCN nanosheets was about 3 nm. Transmission electron microscopy (TEM) images (Figure 2 B, C) of the CCN at increasing magnification show nanosheets with a size of tens of micrometers on a larger scale. The high-magnification TEM image in Figure 2 C confirms that the basic unit of the agglomerates is sheets with a lateral scale ranging from sub-micrometer to several micrometers. Furthermore, the basic sheet tends to bend and its edges are ragged as a result of minimizing the surface-energy of the sheet. High-resolution TEM (HRTEM) was carried out to investigate the detailed information of the CCN, as shown in Figure 2D. There exists many fringes spacing measures ca. 0.324 nm, corresponding to the (002) lattice spacing of the CN. And, the stacking distance of 0.324 nm is evident by the intense electron diffraction ring (inset), proving high partial crystallinity of the nanosheet.

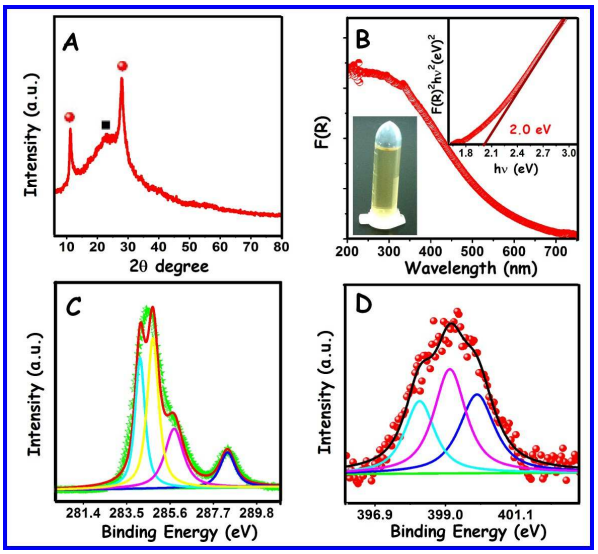

Fig. 3 (A) XRD pattern of CCN; (B) UV-Vis absorption spectra and plots of $(F(R)h\nu)^2$ vs (hν) for the estimation of the optical band gaps of CCN. (C, D) XPS spectra of C 1s and N 1s for CCN.

XRD pattern (Fig. 3A) of CCN that was synthesized by solution synthesis technology present distinctive peaks at 27.48 (d = 3.24 A), corresponding to the (002) interlayer reflection of CN. Moreover, the peaks at 2θ =13° (attributed to the in-planar repeated tri-s-triazine units) shift significantly from 2θ =13° to 2θ =11°(Fig. S3). The broader diffraction peak appeared to be very close to the diffraction peak characteristic to the interplanar spacing of the graphitic structure which appeared at the 2θ of about 26.5°. These results indicated a regular in-planar connection of tri-s-triazine tectons in the C_3N_4 layers, while some degree of disorder may exist in the packing of the C_3N_4 layer, and the aromatic carbon coming from the hydrothermal carbonization of glucose might enlarge the distance among the melon

unites.[10] The evolution of undulation and "curls" during the assembly process in liquid medium may disturb the long-range packing of the C_3N_4 layer along the (002) direction, as reflected already throughout the formation of nanosheet topology at 180 °C. Fourier transformed infrared (FTIR) spectra (Figure S5) of the CN and CCN were characterized by a series of bands in the 900-1800 cm^{-1} region and a strong peak at approximately 800 cm^{-1}. The characteristic IR spectrum of the nanosheets is similar to that of the bulk material. The sharp peak at around 800 cm^{-1} is originated from heptazine ring system. The peaks in the region from 900 to 1800 cm^{-1} are attributed to either trigonal C-N(-C)-C (full condensation) or bridging C-NH-C units. In order to confirm the proposed heptazine structure in the CN framework, ^{13}C MAS NMR analysis (Figure S6) is a more powerful tool. The spectrum of CCN sample shows two distinct peaks at d=164.5 and 156.6 ppm. The first resonance is assigned to the C(e) atoms ($CN_2(NHx)$), whereas the second one was attributed to the C(i) atoms of melem (CN_3). These results support the assembly of CC and MA to the extended aromatic CN framework, which is based on heptazine repeating units.

The UV-visible absorption spectra in Fig. 3B shows an obvious red shift of the intrinsic absorption edge in the nanosheets with respect to the bulk CN. The derived bandgaps from the plots of the $(KM*energy)^n$ (n = 2 for the direct bandgap) versus the energy of the light adsorbed are 2.0 and 2.6 eV for the nanosheets and the bulk material, which could be ascribed to the introduction of carbon doped in CN framework favoring the narrower band gap. The well-defined Tyndall effect of the CCN nanosheet solution as displayed in the inset of Fig. 3B indicates the presence of highly monodisperse ultrathin nanosheets in water. X-ray photoelectron spectroscopy was used to measure the oxidation state of the prepared samples (Fig. 3C, D). High-resolution spectra of C1s at 286.25 eV and N1s at 398.82 eV are

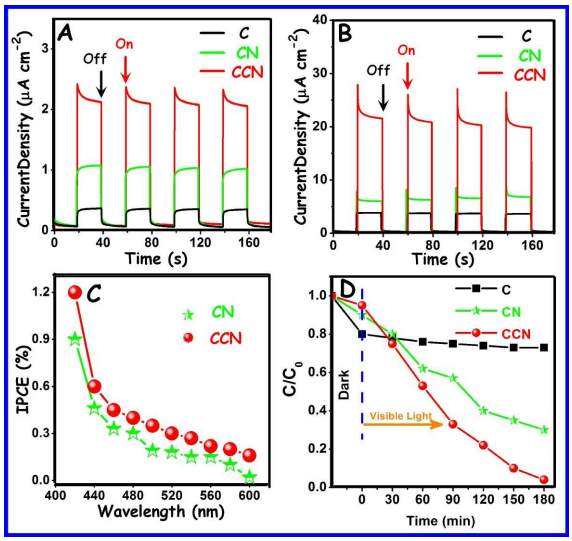

Fig. 4 (A, B) Photocurrents of C, CN and CCN electrodes under visible light irradiation (λ > 400 nm) and under UV irradiation (λ=254 nm); (C) IPCE spectrum of ITO/CN and ITO/CCN biased at -0.2 V vs. Ag/AgCl. (saturated KCl) in 0.1m KCl containing 20 mM $K_4Fe(CN)_6$; (D) Photocatalytic activity of the samples under illumination with visible light.

assigned to the sp^2 C=N bond in the s-triazine ring. The peaks at 288.45 eV and 284.6 eV in the C1s zone are attributed to electrons originating from a sp^2 C atom attached to a $-NH_2$ group and to an aromatic carbon atom. The binding energy with a peak at 284.2 eV was attributed to the accumulation of graphite carbon. The contribution at 399.95 and 400.55 eV in the N1s zone are ascribed to N atoms that are bound to three C atoms; these N atoms are located in the heptazine ring and as bridging atom, respectively. The results support the assembly of glucose and MA to the extended aromatic CN framework, which is largely based on heptazine repeating units.

The photocatalytic activities of the CCN nanosheets were estimated by detecting the photocurrents generated and evaluated by degradation of organic pollutants 4-nitrophenol (4-NP). As shown in Fig. 4 A, B, it was clear that fast and uniform photocurrent responses were observed in both electrodes and the photoresponsive phenomenon was entirely reversible. Under UV light irradiation, the photocurrent of the CCN electrode was about five times as high as that of the CN electrode (Figure 4A). Under visible light irradiation, CN showed almost no photocurrent response. On the contrary, CCN photocatalyst showed a noticeable photocurrent under visible light irradiation (Figure 4B). The photocurrent enhancement of the CCN photocatalyst indicated an enhanced photoinduced electrons and holes separation, which could be attributed to the increase electrical conductivity. Such obviously different electronic conductivity between the bulk CN and CCN nanosheet can be confirmed by the electrochemical impedance spectroscopy (EIS). All the impedance spectra (shown in ESI FigS7) are similar, being composed of one semicircle at high frequency followed by a linear component at low frequency. There are two differences in these curves. Firstly, in the high frequency intercept of the real axis, the internal resistances (R_b) are different. Compared with CN, the R_b of CCN electrode is decreased, suggesting that the carbon-rich system improve the electron conductivity of CN. Secondly, the diffusive resistance (Warburg impedance) of the CCN electrode, represented by the straight line at low frequency, is lower than that of CN. It indicates that the 2D nanosheet structure of the CCN can reduce the mass-transfer resistance and enhance the electrolyte penetration as well as ion diffusion in the host material. What's more, the CCN electrode also shows a smaller charge transfer resistance (Rct), which corresponds to the smaller semicircle in the impedance plots. The low Rb, Rct and Warburg impedance (Table S2) reveal the excellent electrochemical capacitive properties of the carbon-rich material. The incident photon-to-electron conversion (IPCE) spectrum is powerful to quantitatively reveal their photocatalytic activity as a function of wavelength of incident light,which is important to confirm the increased photocatalytic activity. The IPCE spectrum of CCN and CN in Fe^{II} was also performed and is shown in Fig. 4 C. Clearly, the CCN sample significantly improves the photoresponse in the visible light region compared to the CN, which are consistent with their photocurrent data. Since DR spectra, photocurrent and IPCE spectrum clearly showed that the enhanced visible light absorption wavelength of CCN, we hoped that the

samples present photochemical activity in the visible light region. Therefore, we carried out experiments of the photocatalytic degradation of 4-nitrophenol (4-NP) as a test reaction. CCN gives a significantly improved degradation rate compared to CN (Fig. 4D), which could be ascribed to the formation of sheet nanostructure, enhanced light absorption wavelength and increase electrical conductivity promoting charge separation at the interface.

Conclusions

In conclusion, a catalyst-free, solution-processed approach has been developed for the textural engineering of triazine monomers to CN nanomaterials. The as-obtained superstructure possesses a decreased band gap and enhanced light-harvesting capability. The photocatalytic activity of the CCN samples for organic pollutant degradation was greatly improved over the traditional g-CN samples. The photocatalytic and photocurrent activity of CCN samples was comparative to that of g-CN; however the considerable low synthesis temperature without employment of extra catalysts was a breakthrough in CN chemistry. We believe that this innovative assembly route in solution for nanostructured CN at mild conditions will offer a new avenue to construct CN-based semiconductors by integrating this route to diverse approaches for modification in solution at low temperatures. That way, chemical composition, electronic structure, and surface functionality can be much better engineered for advanced applications in the fields of catalysis, energy, and environmental remediation.

Acknowledgements

The present work is supported financially by the National Basic Research Program of China (973 Program) (Grant No. 2012CB933703), the National Natural Science Foundation of China (No. 91233204, 51272041, and 61201107), and the 111 Project (No. B13013), and also financially supported by China Scholarship Council (CSC) and German Academic Exchange Service (DAAD).

Notes and references

[a]*Center for Advanced Optoelectronic Functional Materials Research, and Key Laboratory of UV Light-Emitting Materials and Technology of Ministry of Education, Northeast Normal University (P.R. China) E-mail: clshao@nenu.edu.cn*

[b]*School of Materials Science and Engineering, Zhengzhou University, Zhengzhou 450002 (P.R. China)*

[c] *Institute for Soft Matter and Functional Materials, Helmholtz-Zentrum Berlin fur Materialien und Energie GmbH, Hahn-Meitner-Platz 1, D-14109 Berlin, Germany*

†Electronic Supplementary Information (ESI) available: See DOI: 10.1039/b000000x/

1. (a) X. Wang, K. Maede, A. Thomas, K. Takanabe, G. Xin, J. M. Carsson, K. Domen, M. Antonietti, Nat.Mater. 2009, 8, 76; (b) Y. Wang, J. Yao, H. Li, D. Su, M. Antonietti, J. Am. Chem. Soc. 2011, 133, 2362; (c) Y. Zhang, T. More, J. Ye, M. Antonietti, J. Am. Chem. Soc. 2010, 132, 6294; (d) A. Fischer, M. Antonietti, A. Thomas, Adv. Mater. 2007, 19, 264.
2. (a) Y. Wang, X. Wang, M. Antonietti, Angew. Chem. Int. Ed. 2012, 51, 68; (b) Y. Zheng, J. Liu, J. Liang, M. Jaroniec, S. Qiao, Energy Environ. Sci. 2011, 5, 6717.
3. (a) L. Ge, C. Han, J. Liu, Applied Catalysis B: Environmental 2011, 108, 100; (b) J. Xu, L. Zhang, R. Shi, Y. Zhu, J. Mater. Chem. A 2013, 1, 14766;(c) H. Sun, G. Zhou,Y. Wang, A.Suvorova, S.Wang, ACS Appl. Mater. Interfaces 2014, 6, 16745-16754.
4. (a) Y. Wang, J. S. Zhang, X. C. Wang, M. Antonietti, H. R. Li, Angew. Chem. Int. Ed. 2010, 49, 3356; (b) G. Liu, P. Niu, C. H. Sun, S. C. Smith, Z. G. Chen, G. Q. Lu, H. M. Cheng, J. Am. Chem. Soc. 2010,132, 11642; (c) J. S. Zhang, J. H. Sun, K. Maeda, K. Domen, P. Liu, M. Antonietti, X. Z. Fu, X. C. Wang, Energy Environ. Sci. 2011, 4, 675.
5. (a) X. Zhang, X. Xie, H. Wang, J. Zhang, B. Pan, Y. Xie, J. Am. Chem. Soc. 2013, 135, 18; (b) P. Niu, L. Zhang, G. Liu, H. M. Cheng, Adv. Funct. Mater. 2012, 22, 4763.
6. (a) J. Jiang, K. Zhao, X. Xiao, L. Zhang, J. Am. Chem. Soc. 2012, 134, 4473; (b) Y. Zhu, T. Mei, Y. Wang, Y. Qian, J. Mater. Chem. 2011, 21, 11457.
7. (a) J. Zhang, X. Chen, K. Takanabe, K. Maeda, K. Domen, J. Epping, X. Fu, M. Antonietti, X. Wang, Angew. Chem. 2010, 122, 451; Angew. Chem. Int. Ed. 2010, 49, 441; (b) J. Zhang, M. Zhang, R. Sun, X. Wang, Angew. Chem. 2012, 124, 10292; Angew. Chem. Int. Ed. 2012, 51, 10145; (c) F. Su, S. Mathew, L. Mçhlmann, M. Antonietti, X. Wang, S. Blechert, Angew. Chem. 2011, 123, 683; Angew. Chem. Int. Ed. 2011, 50, 657;(d) Q. Lv, C. Cao, C. Li, J. Zhang, H. Zhu, X. Kong, X. Duan, J. Mater. Chem. 2003, 13, 1241; (e)C. Cao, F. Huang, C. Cao, J. Li, H. Zhu. Chem. Mater., 2004, 16, 5213; (f) Q. Luv, C. Cao, J. Zhang, C. Li, H. Zhu, Applied Physics A, 2004, 79, 633-636.
8. T. Hoheisel, S. Schrettl, R. Szilluweit, H. Frauenrath, Angew. Chem. Int. Ed. 2010, 49, 6496.
9. X. Li, S. Kurasch, U. Kaiser, M. Antonietti, Angew. Chem. Int. Ed. 2012, 51, 9689.
10. Y. Cui, Z. Ding, X. Fu, X. Wang, Angew. Chem. Int. Ed. 2012, 124, 11984.